Journal of Mathematics and Statistics

Research Article

A Mixed Integer Linear Programming for Optimising the Residential Solar Energy Storage System

Teube Cyrille Mbainaissem[1], Dethie Dione[2], Bakary Kone[3] and Youssoupha Toure[2]

[1]*Department of Mathematics and Computer Science, University of N'Djamena, Ndjamena, Chad*
[2]*Department of Formation, SEFS, University of Gaston Berger, Saint-Louis, Senegal*
[3]*Department of Mathematics and Computer Science, University of Felix Houphouet Boigny, Abidjan, Côte D'Ivoire*

Article history
Received: 16-09-2025
Revised: 13-01-2026
Accepted: 15-04-2026

Corresponding Author:
Dethie Dione
Department of Formation, SEFS, University of Gaston Berger, Saint-Louis, Senegal
Email: dethiedione79@gmail.com

Abstract: The global electricity sector is facing a major transition to sustainable energy sources, with consumers playing a crucial role in realising the full potential of the international energy market. Residential energy storage systems are a priority to promote local flexibility and participation in the energy transition. The combination of solar energy generators and storage batteries is a key method of achieving self-sufficiency in residential buildings, thereby increasing individual household independence. A mixed-integer linear programming (MILP) model formulated in AMPL and solved with CPLEX optimizes battery dimensions and operation, thereby improving performance and extending lifespan.

Keywords: Energy Optimisation, Residential Storage, Self-Consumption, Photovoltaic Systems, Intelligent Management, Energy Transition

Introduction

In the 21st century, the lack of electricity is still felt in many villages and towns across underdeveloped, developing, and even developed countries. Yet electricity is now the easiest form of energy to harness. However, before it can be used, it must be produced, transformed, and then transported to consumers. The global energy challenges require greater attention to solar energy (SE), given the difficulties of extending the electricity grid to isolated sites and the environmental and economic drawbacks of fossil fuels. The technological solutions proposed are based on photovoltaic (PV) energy. Over the last few decades, energy concerns and questions have become global issues. It is estimated that almost 80% of the world's total primary energy production comes from fossil fuels, such as oil, gas, and coal, as well as nuclear power (REN21, 2015; Lauinger et al., 2016). These fossil sources are finite and are compounded by the high risk of severe environmental problems, such as global warming and nuclear disasters. The systematic use of fossil fuels results in low production costs but leads to the massive release of greenhouse gases. Fossil fuel-based electricity generation is responsible for almost 40% of the world's CO_2 emissions (Broutin et al., 2009). Solar energy (SE) is more accessible and well-suited to decentralised production, despite its natural and stochastic fluctuations, and it produces cleaner, more environmentally friendly electricity than fossil fuels. Solar energy is among the most abundant renewable energy resources.

Designated as a priority for the coming decades and one of the sub-criteria of the Millennium Development Goals, access to energy is a key challenge for global socio-economic development. Basic human needs, such as water, food, health, and education, will be severely limited without access to electricity. However, access to energy is far from assured in the world's emerging and least developed countries. The major energy production centres are generally located far from the points of consumption. The energy produced is transported over long distances using equipment (transmission lines, line supports, protection equipment along the lines, etc.), which is generally expensive. Control stations are often installed along transmission lines to ensure the continuity and quality of the electrical power transmitted, as well as the voltage and frequency (Macià Cid et al., 2024). In most regions far from major electricity grids, existing power plants are often fueled by fossil fuels, which are costly and polluting.

The cost of extending the electricity network increases gradually with remoteness, whereas fuel prices rise dramatically with isolation. Yet the multiplier effects of access to electricity on human and economic development are undeniable: increases in installed electrical capacity and the growing use of renewable resources could transform economies and ways of life in most countries. According to estimates from the World Bank and the United Nations (UN), 1.3 billion of the planet's 7 billion inhabitants still lack access to electricity. Nearly half of these, 600 million, live in sub-Saharan Africa (two-thirds of the continent's population), around 300 million live in India, and as many in other Asian countries. China has largely resolved its electrification challenges (only 8 million people lack electricity) (Chiacchio et al., 2019). In Latin America, the figure is around 30 million. The electricity market is a particularly complex system, both because of the extensive spread and variety of infrastructure engineering and because of its highly sensitive regulatory framework, which must balance the sources and uses of a precious resource such as energy. Moreover, it is a system in which configurations and infrastructures are constantly evolving and have undergone, and continue to undergo, profound transformations (International Energy Agency-Photovoltaic Energy Systems Programme, 2014). The recent changes in the national energy system, resulting from the rapid spread of renewable sources, mainly photovoltaic, are now necessitating the introduction of new 'intelligent' management and operating methods that actively involve all phases of energy production, distribution, and consumption, to ensure high standards of reliability and safety. In addition, the gradual phase-out of fossil-fuel power stations, with the aim of shutting down all coal-fired generating units by 2025, is reducing essential network services, including voltage and frequency regulation and congestion management. There is therefore a clear need for new decentralised, flexible, and balanced energy systems (Magnor et al., 2009; Biswas et al., 2013).

In particular, the falling cost of energy storage and the growing penetration of renewable energy technologies such as distributed generation integrated into load centres are leading to fundamental changes in the role of energy consumers, paving the way for new entrants to the electricity market, the so-called 'prosumers', because they all consume and produce electricity (Di Somma et al., 2024; Cosic et al., 2021). Prosumers and their assets (distributed generation and storage systems, demand response, electric vehicles, etc.) can interact with one another and with the local distributor or electricity grid, and can be aggregated to form a Local Energy Community (LEC) at the distribution level (GfK Belgium Consortium, 2017; Dias de Lima et al., 2025). In this context, residential neighbourhoods can be seen as the first nucleus for energy communities, aiming to provide active network support by increasing network reliability, flexibility, and resilience.

Investments to promote energy efficiency and the use of renewables as energy sources in buildings, on the one hand, and the increasing deployment of customer-level energy storage systems equipped with Internet of Things (IoT) technologies, such as sensors and smart metering devices, on the other, are therefore identified as key factors enabling the development of energy communities. Distributed smart storage systems can be installed behind the meter alongside local loads, providing flexible energy to a community by reducing the average peak load and increasing self-consumption of local renewables, not only at the individual household level but also at the aggregated community level (Bruce-Konuah & Gupta, 2017; Kulkarni et al., 2017).

In addition, the possibility of exploiting renewable energy sources and moving towards energy self-sufficiency at the community level is a key measure for tackling fuel poverty, as it ensures free access to the electricity market for all community members, including tenants of social housing or multiple-occupancy buildings. In particular, this paper considers a multi-apartment block with ten households living in rented accommodation at a subsidized price as a case study to optimize the storage battery coupled to the photovoltaic generation system, both in terms of sizing and dispatching, to maximize household self-consumption (Lucchetta, 2020; Georgiou et al., 2020; Bordin, 2015).

Solar Energy Storage System

The study focuses on residential consumers who use renewable energy systems such as small-scale solar photovoltaic installations to generate electricity. The objective, as stated in the terms of reference, is to provide information to support policy initiatives on small-scale self-generation for residential consumers. The term 'prosumers' is used broadly to refer to energy consumers who also generate their own energy from various on-site generators; however, this study, as explained above, focuses primarily on residential prosumers who use systems such as small-scale solar PV to generate electricity.

Figure 1 below illustrates the typical solar PV installation on a residential roof with its main components, including the solar PV modules (right), the inverter (the electronic device or circuit that transforms Direct Current (DC) into Alternating Current (AC)), and the house fuse box. In addition, it illustrates the position of the optional storage technology (battery) within the home electricity system, as well as the unique bi-directional meter that can measure current flowing in both directions to and from the grid (net metering).

The photovoltaic system shown in Figure 1 consists of solar panels, an inverter and controller, a storage battery, an electrical load, and a grid connection. The solar panels convert solar radiation into Direct Current (DC), which is then converted to Alternating Current (AC) by the inverter to power the load. The integrated controller manages energy flows among the components. The battery stores excess energy generated by the solar panels for later use, such as at night or during periods of low sunlight. The connection to the electrical grid enables energy importation when solar generation and storage are insufficient and export of surplus energy when production exceeds local demand and storage capacity.

The energy flows within the system are multiple and dynamic. The photovoltaic flow to the load (PV → Load) occurs when the panels directly power the consumers in real time. The photovoltaic flow to the battery (PV → Battery) occurs when production exceeds immediate consumption, enabling storage. The battery-to-load flow (Battery → Load) occurs when solar energy is insufficient, and the battery releases the accumulated energy. Finally, exchanges with the grid (Import/Export) ensure the system's balance: imports cover deficits, while exports monetize surpluses. These mechanisms are orchestrated by the inverter-controller, which continuously optimizes self-consumption, battery life, and economic interactions with the grid.

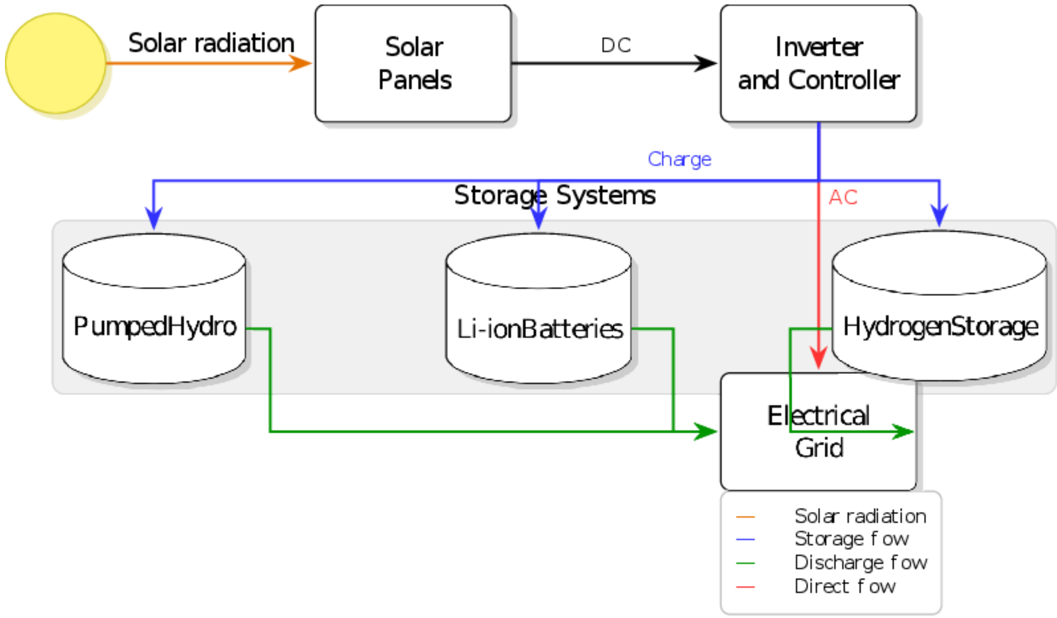

Fig. 1: Solar energy storage programme

Optimisation Model for Battery Management

This section presents the mathematical framework of the mixed-integer linear programming (MILP) model developed to manage residential solar energy storage. It details the model's sets, parameters, and variables, as well as the objective function and the technical constraints that ensure balance between production, consumption, and storage. The equations and logic proposed aim to maximise self-consumption while extending battery life.

Sets and Parameters

The set $\mathcal{B} = \{1 \cdots B\}$ constitutes the types of batteries to be mobilised, indexed by i. $\mathcal{S} = \{1 \cdots S\}$ is the set of time slots indexed by s. It is an ordered set with s_1 being the first time slot. To benefit from annual solar fluxes, the set $\mathcal{T} = \{1 \cdots T\}$ is ordered over the annual period.

The parameter $\delta_{s,t}$ is the solar energy production at time slot s in month t (> 0). The solar energy produced $\nu_{s,t}$ is the total production of solar energy available at time slot s and month t (≥ 0). The minimum and maximum levels for battery i are denoted respectively by γ_i^m, γ_i^M (> 0). The maximum variation for each battery i at time slot s in month t is denoted by $\Delta_{i,s,t}^M$ with (≥ 0). The transfer rate for battery i at time slot s at time t is given by $\tau_{i,s,t}$ with (≥ 0). The minimum solar threshold at time slot s at month t is given by $\beta_{s,t}^m$ (≥ 0). π denotes the penalty for not using a battery ($pi > 0$). M being a sufficiently large constant (> 0).

Variables and Bounds

The continuous variable $b_{s,t}$ is the solar energy demand at time slot s in month t with $\beta_{s,t}^m$ as its lower bound. Thus, we have $b_{s,t} \in [0, \beta_{s,t}^m]$. The binary variable $x_{i,s,t} \in \{0,1\}$ is used to decide whether or not to use a battery i at time slot s in month t. The continuous variable $z_{i,s,t} \in [0, Z]$ denotes the quantity of solar energy charged for battery i at time slot s in month t. The continuous variable $l_{i,s,t} \in [0, L]$ is the amount of solar energy discharged from each battery i at time slot s in month t. The binary variable $r_{i,s,t} \in \{0,1\}$ decides whether or not a battery i is recharged during the time slot s in month t. The continuous variable $y_{i,s,t} \in [\gamma_i^m, \gamma_i^M]$ represents the level of charge of battery i at time slot s in month t. The binary variables $f_{i,s,t}^m, f_{i,s,t}^M \in \{0,1\}$ are indicators of the minimum and maximum battery level i at time slot s in month t. The binary

DOI: 10.3844/jmssp.2026.29.44

variables $f_{i,s,t}^{m}, f_{i,s,t}^{M} \in \{0,1\}$ are indicators of the minimum and maximum battery level i at time slot s in month t. The binary variables $z_{i,s,t}^{m}$, $z_{i,s,t}^{M} \in \{0,1\}$ are auxiliary variables for transitions.

Objective Function and Constraints

The objective function of the model is expressed as follows:

$$\min \left(\sum_{s\in\mathcal{S},t\in\mathcal{T}} b_{s,t} + \pi \sum_{i\in\mathcal{B},s\in\mathcal{S},t\in\mathcal{T}} x_{i,s,t} \right) \tag{1}$$

The first term of (1) relates to the energy cost. It represents the cost of solar energy used at spot s in month t. The second term is the penalty for a delay in recharging with a penalty coefficient π. Minimisation of solar energy: Reduce dependence on solar sources to reduce operational costs and optimise resource use. Penalising installations: Control battery deployment to limit initial investment and avoid overcapacity.

The objective function balances energy and installation costs. The π parameter serves as a weighting factor for this trade-off: If π increases, priority is given to reducing installations; if π decreases, priority is given to saving solar energy. Figure 2 shows the conceptual graphical representation of the objective function.

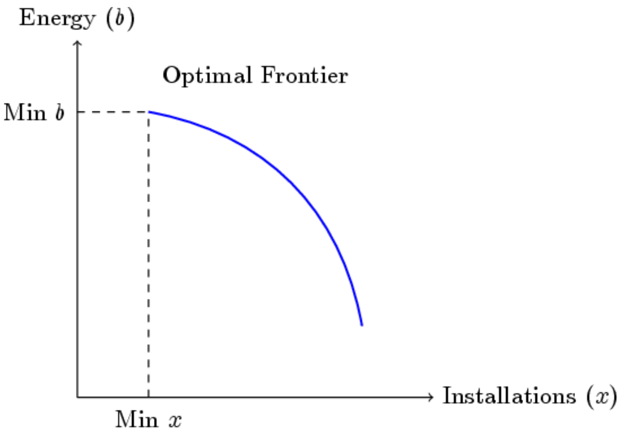

Fig. 2: Conceptual Graphical Representation

$$\sum_{i\in\mathcal{B}} z_{i,s,t} \leq \nu_{s,t} - \delta_{s,t} \quad \forall s \in \mathcal{S}, t \in \mathcal{T} \tag{2}$$

The term $z_{i,s,t}$ refers to the solar energy stored in battery type i during time slot s and month t, while $\nu_{s,t}$ is the total solar energy produced in that period, and $\delta_{s,t}$ represents the surplus energy after meeting demand and discharging. The constraint indicates that the total energy charged into batteries ($\sum z_{i,s,t}$) must not exceed excess solar energy ($\nu_{s,t} - \delta_{s,t}$) to ensure a balance between production, consumption, and storage. Extreme scenarios include: if there is no surplus ($\delta_{s,t} = \nu_{s,t}$), then no energy can be loaded; if all excess is utilized ($\delta_{s,t} = 0$), the total charge is limited to the produced energy ($\sum z_{i,s,t} \leq \nu_{s,t}$). The parameter $\delta_{s,t}$ is influenced by demand and energy discharged, leading to dynamic recalculations of the constraint that, in turn, indirectly minimize energy costs and penalties. For example, with solar production at 20 kWh and unused energy at 5 kWh, efficient resource management ensures immediate demand satisfaction while optimizing the balance between direct consumption and storage. The constraint is vital for preventing battery overcharging and maximizing system efficiency, in conjunction with other constraints, to enable coherent optimization.

$$z_{i,s_1,t} = 0 \quad \forall i \in \mathcal{B}, t \in \mathcal{T} \tag{3}$$

The term $z_{i,s_1,t}$ represents the solar energy charged in battery type i during the first time slot s_1 of month t. Constraint (3) prohibits energy charging during s_1 to initialize a neutral battery state, preventing edge effects between months. Consequently, batteries can only be charged during subsequent time slots. Specifically, for $s = s_1$, it assures $z_{i,s_1,t} = 0$, leading to $l_{i,s_1,t} = 0$, which means load level $y_{i,s_1,t}$ relies solely on the transfer rate $\tau_{i,s_1,t}$ and the previous level. This promotes gradual optimization during the month. For instance, in January (first slot s_1), $z_{1,s_1,\text{January}} = 0$ leads to charging after $01h - 02h$. This method prevents initialization conflicts and supports a consistent system restart each month, aiding long-term optimization through collaborative constraints.

$$\delta_{s,t} = \nu_{s,t} - b_{s,t} - \sum_{i\in\mathcal{B}} l_{i,s,t} \quad \forall s \in \mathcal{S}, t \in \mathcal{T} \tag{4}$$

The term $\delta_{s,t}$ represents unused solar energy at time slot s and month t, while $\nu_{s,t}$ indicates total solar energy production, and $b_{s,t}$ reflects direct solar energy demand. The energy discharged from battery i to meet demand is denoted as $l_{i,s,t}$. The constraint (4) ensures that total solar production equals direct demand plus energy from storage and surplus, thereby balancing all produced energy for efficient utilization or storage. By calculating $\delta_{s,t}$, this framework minimizes excess solar energy, encouraging its sale or storage when surplus exists. Overall, constraint (4) is crucial for optimizing energy use and reducing waste in the system by improving self-consumption, alongside other storage-related constraints.

$$\sum_{t\in\mathcal{T}} y_{i,s_1,t} \leq \gamma_i^M \quad \forall i \in \mathcal{B} \tag{5}$$

The term $y_{i,s_1,t}$ represents the charge level of battery i at time slot s_1 of month t, while γ^{M_i} denotes its maximum capacity. Constraint (5) limits the total initial charge levels across months to not exceed this maximum capacity, ensuring long-term capacity maintenance, preventing overcharging, and aligning with load management constraints. Additionally, (5) provides a global limit, complemented by local variation limits given in (7), thereby facilitating long-term planning, preventive maintenance, and financial optimization. For example, if a battery's capacity is 100 kWh over 12 months, the initial monthly charges must not exceed this capacity. Thus, the constraint mitigates overload risk, complements existing limits, and supports long-term strategic planning.

$$r_{i,s_1,t} = 0 \quad \forall i \in \mathcal{B}, t \in \mathcal{T} \tag{6}$$

The term $r_{i,s_1,t}$ refers to a binary variable indicating if battery i is in recharge mode during the first time slot s_1 of month t. The constraint (6) requires that no battery enter recharge mode during this time slot, consistent with constraint (3), which asserts that no recharging implies no charged energy. Additionally, it interacts with constraint (15), limiting discharge possibilities as $r_{i,s_1,t} = 0$. This ensures numerical stability at the start of each period, promoting sustainable energy management by avoiding conflicts and maintaining physical realism during maintenance or measurement periods. For example, in January's first slot (00h-01h), $r_{1,\text{00h-01h,January}} = 0$, indicating recharging is not allowed, requiring pre-planned recharging thereafter. Overall, constraint (6) facilitates clean system initialization, controls charging sequences, and maintains architectural compatibility.

$$y_{i,s,t} - y_{i,s-1,t} \leq \Delta^M_{i,s,t} \quad \forall i \in \mathcal{B}, t \in \mathcal{T}, s \in \mathcal{S} \setminus \{s_1\} \tag{7}$$

$$-\Delta^M_{i,s,t} \leq y_{i,s,t} - y_{i,s-1,t} \quad \forall i \in \mathcal{B}, t \in \mathcal{T}, s \in \mathcal{S} \setminus \{s_1\} \tag{8}$$

These two constraints govern the variation in the battery's hourly charging rate, specifically constraints (7) and (8). The upper limit is set at $\Delta^M_{i,s,t}$ and the lower at $-\Delta^M_{i,s,t}$, which leads to an absolute variation of $|y_{i,s,t} - y_{i,s-1,t}| \leq \Delta^M_{i,s,t}$. Here, $y_{i,s,t}$ represents the battery charge level at time slot s and month t, while $\Delta^{M_{i,s,t}}$ indicates the maximum allowable variation in kWh/hour. These safeguards prevent sudden changes that could harm battery life and ensure network stability against power fluctuations. For instance, a lithium-ion battery might have $\Delta^M_{1,s,t} = 2\text{kWh/hour}$ with a previous charge of $y_{1,s-1,t} = 5\text{kWh}$, resulting in a permissible range of $3\text{ kWh} \leq y_{1,s,t} \leq 7\text{kWh}$. Overall, the constraints limit the charging and discharging processes to ensure safety and stability within practical technological parameters.

$$\textstyle\sum_{s\in\mathcal{S}} x_{i,s,t} \leq \sum_{s\in\mathcal{S}} (\gamma^M_i - y_{i,s,t}) \quad \forall i \in \mathcal{B}, t \in \mathcal{T} \tag{9}$$

The variables $x_{i,s,t}$ and $y_{i,s,t}$ represent the use and charge level of battery i in time slot s of month t, respectively, with γ^{M_i} indicating the maximum capacity. The (9) constraint limits battery usage to its residual capacity over all time slots, preventing overuse and ensuring that usage aligns with available capacity. For example, if a battery has a maximum of 100 kWh and an average charge of 60 kWh, the constraint allows for a total usage of up to 28,800 kWh across 720 time slots. This approach supports battery lifetime management, optimal sizing, and energy load distribution. Techniques related to this constraint are detailed in Table 1.

Table 1: Technical characteristics of the constraint (9)

Aspect	Description
Type of constraint	Mixed linear (combination of continuous and binary variables)
Physical meaning	Limits total transferable energy
Impact on solution	reduces the space of possible solutions
Relationship to objective	Helps minimise user costs

The constraint (9) serves three essential roles: controlling overall battery use, preventing oversizing, and coordinating instantaneous use with long-term capacity. It is particularly important in high-interruption scenarios for renewable sources, where storage resource management must be rigorously optimized.

$$y_{i,s,t} = \tau_{i,s,t} y_{i,s-1,t} + l_{i,s,t} \quad \forall i \in \mathcal{B}, t \in \mathcal{T}, s \in \mathcal{S} \setminus \{s_1\} \tag{10}$$

The term $y_{i,s,t}$ represents the battery charge level of battery i at slot s of month t, while $y_{i,s-1,t}$ indicates the previous slot's charge. The charge retention rate is denoted by $tau_{i,s,t}$, and the discharged energy is represented by $l_{i,s,t}$. Constraint (10) illustrates the dynamic evolution of battery charge, factoring in the retained charge after losses ($\tau_{i,s,t} y_{i,s-1,t}$) and the current discharge ($l_{i,s,t}$), with recursion based on the previous slot. The discharge $l_{i,s,t}$ is limited by other constraints, exemplified by a lithium-ion battery ($i = 1$), where a retention rate of $\tau_{1,s,t} = 0.99$ and an initial charge of $y_{1,s-1,t} = 50\text{kWh}$ results in $l_{1,s,t} = 5\text{kWh}$ and a subsequent charge of $y_{1,s,t} = 54.5\text{kWh}$. Effective management of losses and model accuracy is crucial for optimizing battery performance.

$$l_{i,s,t} \leq M r_{i,s-1,t} \quad \forall i \in \mathcal{B}, t \in \mathcal{T}, s \in \mathcal{S} \setminus \{s_1\} \tag{11}$$

$$l_{i,s,t} \leq z_{i,s,t} \quad \forall i \in \mathcal{B}, s \in \mathcal{S}, t \in \mathcal{T} \tag{12}$$

$$l_{i,s,t} \geq z_{i,s,t} - M(1 - r_{i,s-1,t}) \quad \forall i \in \mathcal{B}, t \in \mathcal{T}, s \in \mathcal{S} \setminus \{s_1\} \tag{13}$$

The term $l_{i,s,t}$ denotes the energy discharged from battery i at slot s, the term $r_{i,s,t}$ being a binary recharge decision variable, the term $z_{i,s,t}$ indicates the energy available for discharge and M is a sufficiently large constant (Big-M). The constraint (11) activates discharge only if recharge was active in the previous step; the constraint (12) limits discharge to the available energy; and the constraint (13) forces discharge if recharge was active. Table 2 gives the combined logic of these constraints:

Table 2: Combined effects of constraints (11)-(13)

$r_{i,s-1,t}$	Condition	Effect on $l_{i,s,t}$
0	Not reloaded	$0 \leq l_{i,s,t} \leq 0$ (blocked discharge)
\ 1	Recharged	$z_{i,s,t} \leq l_{i,s,t} \leq z_{i,s,t}$ (forced discharge)

The constraints (11)-(13) govern the term $l_{i,s,t}$ of the constraint and ensure $l_{i,s_1,t} = 0$. In a battery scenario where $M = 1000\text{kWh}$ and $z_{1,s,t} = 5\text{kWh}$, two cases arise based on the previous recharge state: if $r_{1,s-1,t} = 0$, then $l_{1,s,t} = 0\text{kWh}$ (blocked); if $r_{1,s-1,t} = 1$, then $l_{1,s,t} = 5\text{kWh}$ (forced). This precise control facilitates charge/discharge synchronization and prevents inconsistent states by ensuring that M exceeds any possible $z_{i,s,t}$. The formulated constraints synthesize the logical coupling with prior states, energy availability, and minimum discharge, positioning this as a classical Big-M system in mixed linear programming, where M must balance the constraints and numerical stability, ideally set to $M = \gamma_i^M$ (the maximum battery capacity).

$$y_{i,s,t} - \gamma_i^m \leq M f_{i,s,t}^m \quad \forall i \in \mathcal{B}, s \in \mathcal{S}, t \in \mathcal{T} \tag{14}$$

$$\gamma_i^M - y_{i,s,t} \leq M f_{i,s,t}^M \quad \forall i \in \mathcal{B}, s \in \mathcal{S}, t \in \mathcal{T} \tag{15}$$

The variable $y_{i,s,t}$ represents the current battery charge level, while γ^{m_i} and γ^{M_i} indicate the minimum and maximum permissible levels, respectively. The binary indicators $f^{m_{i,s,t}}$ and $f^{M_{i,s,t}}$ denote whether the battery charge is not at the minimum or maximum level, with a 'Big-M' constant M applied. Specifically, $f^{m_{i,s,t}} = 1$ if the charge is close to the minimum ($y_{i,s,t} \leq \gamma_i^m + \epsilon$), and $f^{M_{i,s,t}} = 1$ if the charge is close to the maximum ($y_{i,s,t} \geq \gamma_i^M - \epsilon$). The common objective is to detect critical situations to avoid overcharging (equipment protection) and deep discharge (preservation of service life). The Big-M mechanism is given by Table 3, showing the combination of constraints.

Table 3: Combined Operation of Constraints

Condition	Constraint	Effect
$y_{i,s,t} \approx \gamma_i^m$	(14)	Force $f_{i,s,t}^m = 1$
$y_{i,s,t} \approx \gamma_i^M$	(15)	Force $f_{i,s,t}^M = 1$
Other cases	Both	Leave the indicators at 0

The indicators specified in equations (14)-(15) dictate recharging decisions influenced by constraints (7)-(8). The limits γ_i^m and γ_i^M determine the permissible $\Delta_{i,s,t}^M$. For a lithium-ion battery, $\gamma_i^m = 10kWh$ (20% capacity) and $\gamma_i^M = 50kWh$ (100% capacity) for $M = 100$ kWh. This leads to different cases for the allowed energy outputs, establishing binary-variable constraints that should be used judiciously. The optimization of these constraints, particularly choosing M as $1.2 \times \gamma_i^M$, is crucial for effectively managing the recharging process, as shown in Table 4.

Table 4: Summary of constraints (14)-(15)

Aspect	Constraint (14)	Constraint (15)
Protection	Against deep discharge	Against overload
Indicator variable	$f_{i,s,t}^m$	$f_{i,s,t}^M$
Critical threshold	γ_i^m	γ_i^M

These constraints are crucial for systems with expensive batteries, critical applications where availability is paramount, and battery lifespan models.

$$r_{i,s,t} \leq 1 - f_{i,s,t}^m \quad \forall i \in \mathcal{B}, s \in \mathcal{S}, t \in \mathcal{T} \tag{16}$$

$$r_{i,s,t} \geq 1 - f_{i,s,t}^M \quad \forall i \in \mathcal{B}, s \in \mathcal{S}, t \in \mathcal{T} \tag{17}$$

We have binary variables related to battery recharge decisions. It defines $r_{i,s,t}$ as the recharge decision, with $f^{m_{i,s,t}}$ representing a minimal level and $f^{M_{i,s,t}}$ indicating a maximal level. Two constraints govern these decisions: one blocks recharging when the battery is nearly empty, and another requires recharging when it is almost full. The objective is to maintain the battery charge within an optimal operating zone; Table 5 lists the indicator states.

Table 5: Possible combinations of indicators

$f_{i,s,t}^m$	$f_{i,s,t}^M$	$r_{i,s,t}$ via (16)	$r_{i,s,t}$ via (17)
0	0	≤ 1	$\geq 1 \Rightarrow$ free
1	0	≤ 0	$\geq 1 \Rightarrow$ impossible
0	1	≤ 1	$\geq 0 \Rightarrow$ free
1	1	≤ 0	$\geq 0 \Rightarrow r_{i,s,t} = 0$

The indicators $f_{i,s,t}^m$ and $f_{i,s,t}^M$ are derived from constraints for level detection. The decision $r_{i,s,t}$ impacts $l_{i,s,t}$ via specific constraints, particularly with charge evolution considerations. For battery i in case 1, a critical level ($f^m = 1$, $f^M = 0$) creates scenarios that result in inconsistencies. Conversely, case 2 denotes a normal level ($f^m = 0$, $f^M = 0$), and case 3 indicates a high level ($f^m = 0$, $f^M = 1$). Strategies are implemented to prevent dangerous charge states, optimize efficiency, and enhance durability, as detailed in Table 6, which outlines behaviors under different charging conditions and the corresponding actions.

Table 6: Summary of Different Charging Situations

Situation	Authorized Charging	Typical Action
Too low level ($f^m = 1$)	No	Disconnection
Optimal level	Yes	Normal recharge
High level ($f^M = 1$)	Optional	Maintenance or use

For more precise management, it is necessary to impose a minimum charging duration constraint to introduce differential costs based on the charge level and to account for cycle history.

$$(1 - f^m_{i,s,t}) - (1 - f^m_{i,s-1,t}) \leq z^m_{i,s,t} \quad \forall i \in \mathcal{B}, t \in \mathcal{T}, s \in \mathcal{S} \setminus \{S_1\} \quad (18)$$

$$z^m_{i,s,t} \geq f^m_{i,s,t} - f^m_{i,s-1,t} \quad \forall i \in \mathcal{B}, t \in \mathcal{T}, s \in \mathcal{S} \setminus \{S_1\} \quad (19)$$

Remark 1

The variable $z^m_{i,s,t}$ detects transitions of the minimum level indicator $f^m_{i,s,t}$:

$$z^m_{i,s,t} = \begin{cases} 1 & \text{if } f^m_{i,s-1,t} = 0 \text{ and } f^m_{i,s,t} = 1 \text{ (entry into critical zone)} \\ 1 & \text{if } f^m_{i,s-1,t} = 1 \text{ and } f^m_{i,s,t} = 0 \text{ (exit from critical zone)} \\ 0 & \text{Otherwise} \end{cases}$$

The binary indicator variable $f^{m_{i,s,t}}$ represents the minimal level constraint, while $z^{m_{i,s,t}}$ denotes a binary transition variable. The goal is to monitor the battery's entry and exit from the low critical zone. Constraint (18) signifies the transition from $f^m = 0$ to $f^m = 1$, and Constraint (19) identifies any change in the indicator. Together, these constraints enable precise detection of entry ($0 \to 1$) and exit ($\to 0$) transitions from the critical zone, as summarized in Table 7.

Table 7: Combined effect of constraints (18)-(19)

$f^m_{i,s-1,t}$	$f^m_{i,s,t}$	$z^m_{i,s,t}$ via (18)	$z^m_{i,s,t}$ via (19)
0	0	≤ 0	$\geq 0 \Rightarrow 0$
0	1	≤ 1	$\geq 1 \Rightarrow 1$
1	0	≤ -1	$\geq -1 \Rightarrow 0$
1	1	≤ 0	$\geq 0 \Rightarrow 0$

The document discusses the minimum-level detection of input signals for specific constraints, detailing how the Recharge control influences recharge decisions based on detected transitions. For battery i, a normal level is represented as $f^m_{i,s-1,t} = 0$ and a critical level as $f^m_{i,s,t} = 1$. This leads to a calculated transition value of $z^m_{i,s,t} = 1$. Furthermore, predictive maintenance emphasizes counting entries into critical zones and employs optimization strategies that penalize frequent transitions to facilitate early problem detection. A summary of different behaviors with respect to transitions is provided in Table 8.

Table 8: Summary of the Different Transitions

Transition	$z^{m_{i,s,t}}$	Signification
Stable out of critical condition ($0 \to 0$)	0	Normal
Entry into critical condition ($0 \to 1$)	1	Alert
Exit from critical condition ($1 \to 0$)	0	Recovery
Stable in critical condition ($1 \to 1$)	0	Persistent problem

These constraints limit the number of critical transitions, impose costs on entering critical zones, and record the history of critical states.

$$(1 - f^M_{i,s,t}) - (1 - f^M_{i,s-1,t}) \leq z^M_{i,s,t} \quad \forall i \in \mathcal{B}, t \in \mathcal{T}, s \in \mathcal{S} \setminus \{S_1\} \quad (20)$$

$$z^M_{i,s,t} \geq f^M_{i,s,t} - f^M_{i,s-1,t} \quad \forall i \in \mathcal{B}, t \in \mathcal{T}, s \in \mathcal{S} \setminus \{S_1\} \quad (21)$$

The term $f^{M_{i,s,t}}$ is the indicator variable for the maximum level (of constraint 15), and the term $z^{M_{i,s,t}}$ is the binary transition variable. The objective is to detect changes in the state of the maximum load indicator. Constraint (20) captures the transition $0 \to 1$ (entry into the critical zone). Constraint (21) captures the transition $\to 0$ (exit from the critical zone). Together, they detect all the changes in the indicator f^M. Table 9 shows the detection logic.

Table 9: Detection of maximum charge indicator transitions

$f^M_{i,s-1,t}$	$f^M_{i,s,t}$	$z^M_{i,s,t}$ via (20)	$z^M_{i,s,t}$ via (21)
0	0	≤ 0	$\geq 0 \Rightarrow 0$
0	1	≤ 1	$\geq 1 \Rightarrow 1$
1	0	≤ -1	$\geq -1 \Rightarrow 0$
1	1	≤ 0	$\geq 0 \Rightarrow 0$

With respect to the defined indicator f^M, the analysis of equations (20) and (21) is central to recharge control, where detected transitions inform recharge decisions. For instance, the battery scenario $i = 1$ indicates a transition from a normal level to a critical level. The application of constraints shows that certain conditions lead to detected transitions, enabling predictive maintenance that optimizes detection of critical states while penalizing frequent transitions. Constraint (20) focuses on maximum-load activation detection, while Constraint (21) addresses maximum-load deactivation detection. Overall, these constraints facilitate tracking charge states, implement nonlinear transition costs, and enhance battery longevity through adaptive control.

Proposition 1

The total amount of solar energy charged across all batteries, time slots, and months is bounded above by the product of the number of batteries, the number of time slots, the number of months, and the upper bound of the charge variable. Formally:

$$\sum_{i \in \mathcal{B}} \sum_{s \in \mathcal{S}} \sum_{t \in \mathcal{T}} z_{i,s,t} \leq B \times S \times T \times Z$$

where :

- $B = |\mathcal{B}|$ (number of batteries)
- $S = |\mathcal{S}|$ (number of time slots)
- $T = |\mathcal{T}|$ (number of months)
- Z is the upper bound of the variable $z_{i,s,t} \in [0, Z]$

Proof

$$z_{i,s,t} \leq Z \quad \forall i, s, t$$

$$\Longrightarrow \sum_i \sum_s \sum_t z_{i,s,t} \leq \sum_i \sum_s \sum_t Z$$

$$\leq Z \times \sum_i \sum_s \sum_t 1$$

$$\leq Z \times (B \times S \times T)$$

The proof follows directly from the definitions of the variable bounds and the summation of the inequalities. This upper bound is crucial for:

1. Capacity analysis: It provides a theoretical upper limit on the total energy that can be stored over the considered period.
2. Resource planning: It allows for the sizing of the necessary storage infrastructure to cope with maximum solar production. It enables sizing the necessary storage infrastructure to accommodate peak solar production.
3. Performance evaluation: Performance evaluation: By comparing the actual value of the energy stored at this terminal, we can evaluate the efficiency of the use of storage capacities.

Proposition 2

The total charge level of all batteries at any given time is capped by the sum of their individual maximum capacities. If we denote $Y_{\max}$ as the maximum total charge level of the system:

$$Y_{\max} \leq \sum_{i \in \mathcal{B}} \gamma_i^M$$

where γ_i^M is the maximum capacity of battery i.

Proof

Let's consider the instantaneous charge level of each battery i at slot s and month t:

$$y_{i,s,t} \leq \gamma_i^M \quad \forall i, s, t$$

The total load level of the system at this moment is therefore:

$$\sum_{i \in \mathcal{B}} y_{i,s,t} \leq \sum_{i \in \mathcal{B}} \gamma_i^M$$

This inequality being valid for any instant (s, t), the maximum total charge level $Y_{\max}$ necessarily satisfies:

$$Y_{\max} \leq \sum_{i \in \mathcal{B}} \gamma_i^M$$

1. System security: This terminal ensures that the total charge level will never exceed the total physical capacity of the batteries, thus avoiding the risk of overcharging.
2. System sizing: It allows for the determination of the total storage capacity needed to meet the energy demand.
3. Economic optimization: Economic optimization: By knowing this limit, we can optimize investment in storage capacities by avoiding oversizing. By knowing this benchmark, we can optimize investment in storage capacity by avoiding overestimation.

Numerical Results

The set of batteries $\mathcal{B} = \{B_1, B_2, B_3\}$ where $B_i \in \mathcal{B}$ represents a battery. The set of time slots $\mathcal{S} = \{S_1, S_2, S_3, S_4\}$ with $S_j \in \mathcal{S}$ represents a time slot. The model was tested for over 1 year in AMPL and solved by CPLEX 22.1.1.0, yielding an optimal integer solution with an objective of 36844.6 and 20 MIP simplex iterations. Thus, the set of months is $\mathcal{T} = \{t_1, \ldots, t_{12}\}$ where $t_k \in \mathcal{T}$ represents a month.

Table 10 (Amorosi et al., 2022) summarizes the parameters of the battery system. With 3 batteries of 4 kWh, the total gross capacity is 12 kWh, but the useful operating range is 20 % to 80 % SOC, for a usable capacity of 28.8 kWh. The initial state of charge is 2.8 kWh (approximately 5.8% of the total capacity). The charge and discharge rates of 2 kW/h per battery add up to a total power of 24 kW. These parameters are typical for optimizing battery lifespan while ensuring adequate storage capacity.

Table 10: Summary of technical input parameters for the optimization model

Battery storage system parameters	
Battery capacity	4 kWh
Number of batteries (initial assumption)	3
Battery minimum state of charge	20%
Battery maximum state of charge	80%
Initial state of charge	2.8 kWh
Charge rate	2 kW/h
Discharge rate	2 kW/h

Demand is consistently higher in the evening (S4) and lower at night (S1). Each time slot follows the same monthly progression (+5 kWh/month). The gap between time slots remains constant throughout the year. Table 11, composed of two sub-tables, provides assumed data on the monthly energy demand by time slot (in kWh).

Table 11: Monthly energy demand by time slot (in kWh)

Time slot	Month											
	Jan	Feb	Mar	Apr	May	Jun	Jul	Aug	Sep	Oct	Nov	Dec
S1 (00h-06h)	100	105	110	115	120	125	130	135	140	145	150	155
S2 (06h-12h)	150	155	160	165	170	175	180	185	190	195	200	205
S3 (12h-18h)	200	205	210	215	220	225	230	235	240	245	250	255
S4 (18h-24h)	250	255	260	265	270	275	280	285	290	295	300	305

S1 *: Night (00h-06h) - Lowest demand*
S2 *: Morning (06h-12h) - Gradual increase*
S3 *: Afternoon (12h-18h) - Intermediate period*
S4 *: Evening (18h-24h) - Peak demand*
Trend *: +5 kWh/Month for all the time slots*

A 60 V difference between each time slot represents a constant gap. A steady growth with a linear monthly increase of 5 V. A diurnal variation with an amplitude of 160 V between night and evening. Tables 12 and 13 provide assumed relationships with energy demand and monthly available voltage by time slot (in volts).

The voltage follows the same time progression as the energy demand. The differences between slots are stable throughout the year. Transformers need to be adjusted according to time slots.

Table 12: Monthly available voltage per time slot (in volts)

Time slot	Month											
	Jan	Feb	Mar	Apr	May	Jun	Jul	Aug	Sep	Oct	Nov	Dec
S1 (00h-06h)	120	125	130	135	140	145	150	155	160	165	170	175
S2 (06h-12h)	180	185	190	195	200	205	210	215	220	225	230	235
S3 (12h-18h)	220	225	230	235	240	245	250	255	260	265	270	275
S4 (18h-24h)	280	285	290	295	300	305	310	315	320	325	330	335

S1 *: Night - Lowest tension*
S2 *: Morning - Gradual increase*
S3 *: Afternoon - Intermediate level*
S4 *: Evening - Maximum tension*
Trend *: +5\,V/month for all time slots*

Table 13: Voltage/demand matching

Time slot	Voltage (V)	Demand (kWh)
S1 (00h-06h)	120-175	100-155
S2 (06h-12h)	180-235	150-205
S3 (12h-18h)	220-275	200-255
S4 (18h-24h)	280-335	250-305

Energy Demand Table

Through Table 14 of the results (in kWh), we noted the main trends in energy demand. Indeed, morning demand remained stable, with S1 (20 kWh) and S2 (30 kWh) remaining constant throughout the year. In addition, there is a diurnal variation with a peak in July for S3 (12 kWh) and S4 (14 kWh) and a minimum in winter for S3 (8 kWh) and S4 (8.6-10 kWh). Significant values such as $\Delta_{\max} = 14\,\text{kWh (S4/Jul)} - 8\,\text{kWh (S3/Jan)} = 6\,\text{kWh}$ are thus obtained as results. The relationships with the other parameters are summarised in the following formula:

$$b_{s,t} \in [\beta^m_{s,t}, \nu_{s,t} - \delta_{s,t}]$$

where $\beta^m_{s,t}$ is the minimum deficit and $\nu_{s,t}$ is the solar production.

Table 14: Solar energy demand by time slot and month (in kWh)

Months	S1 (00h-06h)	S2 (06h-12h)	S3 (12h-18h)	S4 (18h-24h)
Jan	20	30	8.0	8.6
Feb	20	30	8.0	9.0
Mar	20	30	8.0	10.0
Apr	20	30	9.0	11.0
May	20	30	10.0	12.0
Jun	20	30	11.0	13.0
Jul	20	30	12.0	14.0
Aug	20	30	11.0	13.0
Sep	20	30	10.0	12.0
Oct	20	30	9.0	11.0
Nov	20	30	8.0	10.0
Dec	20	30	8.0	9.0

We have identified the implications for the model. Thus, the constraints associated with this table of results are the equilibrium constraints (2) and the dimensioning constraints (4). The dimensioning provides for the capacity to cover S4 in July (14 kWh), with optimisation to adapt storage strategies to the seasonality of the S3-S4 slots, to obtain specific monitoring of the April-May and August-September transitions. Table 15 shows the correspondence with the system parameters. The variable $b_{s,t}$ represents the share of demand directly met by solar energy, which must comply with the lower bound $\beta^m_{s,t}$ (minimum deficit) and the actual availability $\nu_{s,t}$ (solar production).

Table 15: Correspondence with system settings

Time slots	Request Type	Critical Period
S1	Base charge	Stable night
S2	Morning charge	Constant morning
S3	Seasonal variation	Summer afternoon
S4	Evening peak	Summer evening

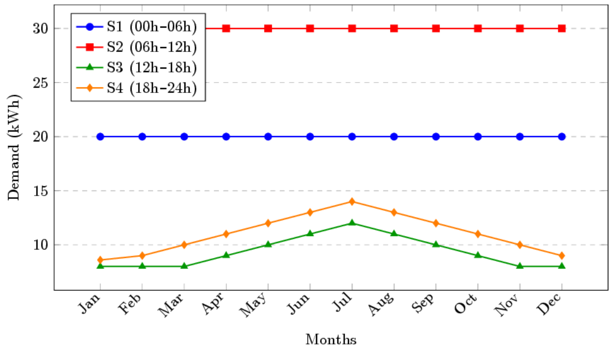

Fig. 3: Monthly solar energy demand by time slot

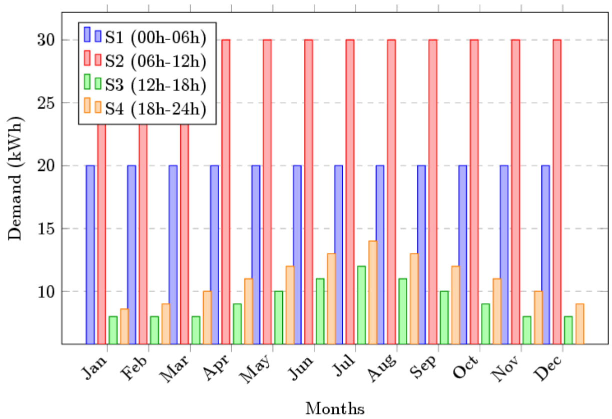

Fig. 4: Bar chart comparison of time slots

This study examines the monthly evolution of solar energy demand across four time slots, utilizing three visual formats to illustrate seasonal trends. Figure 3 indicates that slots S1 (00h-06h) and S2 (06h-12h) maintain constant demands of 20 kWh and 30 kWh, respectively, while slots S3 (12h-18h) and S4 (18h-24h) display seasonal variations characterized by a sinusoidal pattern. Minimum demand occurs in winter (8 kWh for S3 and 8.6 kWh for S4 in January), and maximum demand occurs in summer (12 kWh for S3 and 14 kWh for S4 in July). A bar chart in Figure 4 highlights the dominance of S2, which is 50% more energy-intensive than S1, resulting in a stable hierarchy of $S2 > S1 >$

DOI: 10.3844/jmssp.2026.29.44

$S4 > S3$ throughout the year. Notable convergence occurs in the winter months, as demand for S3 and S4 aligns. Figure 5 quantifies the seasonal variation amplitudes, detailed in Table 16.

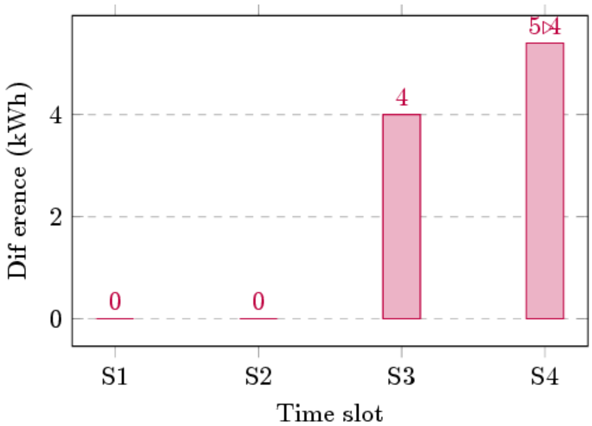

Fig. 5: Difference between minimum and maximum values over the year

Table 16: Seasonal variation range

Time slot	Difference (kWh)	Relative variation
S1	0	0%
S2	0	0%
S3	4	+50% (812)
S4	5.4	+63% (8.614)

Several lessons emerge from this analysis. Night-time stability (S1) shows a constant demand, suggesting regular use (e.g., refrigeration, electronic devices left on standby). A morning peak (S2) probably corresponds to households waking up (heating, hot water, morning preparations). Diurnal sensitivity (S3-S4) varies with sunlight, for example, in summer, when air conditioning and prolonged activities are prevalent, and in winter, when early nights reduce demand. This analysis reveals a fundamental dichotomy between rigid slots (S1-S2) linked to biological rhythms and flexible slots (S3-S4) dependent on climatic conditions. These insights could guide seasonal energy management policies, particularly for sizing storage capacities.

Batteries Usage Matrices

Table 17 highlights three key traits of the energy management system: uniform battery activation indicates a centralized approach, while slot S2 remains inactive, suggesting underutilization during that timeframe. Seasonal trends indicate significant use of slot S1 at extreme temperatures and predominant activity in slot S3 during the off-seasons, with minimal engagement of slot S4. Figure 6 reveals that S3 accounts for 50% of activations, cementing its role, while S1 deals with critical demands. The data indicate opportunities for improved management, particularly by addressing the inactive S2 and underutilized S4, which could lead to system consolidation and increased utilization of storage capacity.

Table 17: Battery usage schedule (1 = enabled, 0 = disabled)

Time slot	Month											
	Jan	Feb	Mar	Apr	May	Jun	Jul	Aug	Sep	Oct	Nov	Dec
B1-S1	1	0	0	0	1	0	0	1	0	0	0	1
B1-S2	0	0	0	0	0	0	0	0	0	0	0	0
B1-S3	0	1	0	1	0	1	1	0	1	0	1	0
B1-S4	0	0	1	0	0	0	0	0	0	1	0	0
B2-S1	1	0	0	0	1	0	0	1	0	0	0	1
B2-S2	0	0	0	0	0	0	0	0	0	0	0	0
B2-S3	0	1	0	1	0	1	1	0	1	0	1	0
B2-S4	0	0	1	0	0	0	0	0	0	1	0	0
B3-S1	1	0	0	0	1	0	0	1	0	0	0	1
B3-S2	0	0	0	0	0	0	0	0	0	0	0	0
B3-S3	0	1	0	1	0	1	1	0	1	0	1	0
B3-S4	0	0	1	0	0	0	0	0	0	1	0	0

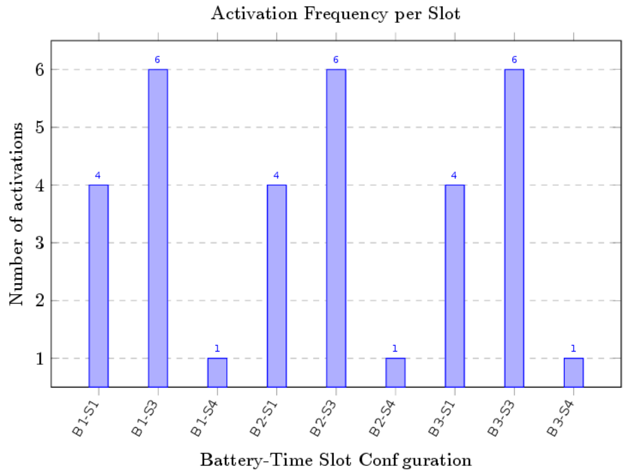

Fig. 6: Number of monthly activations per configuration

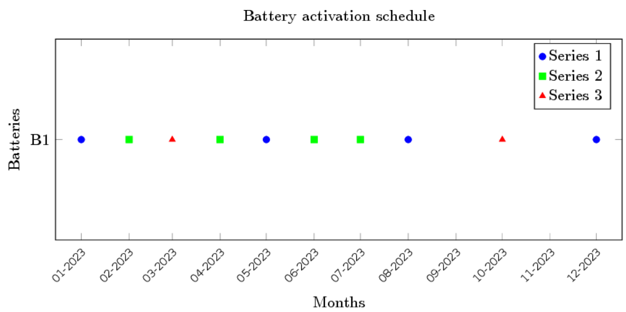

Fig. 7: Battery activation schedule B1

Table 18: Summary of activation strategies

Period	Active Slot	Frequency
Winter	S1	33%
Spring/Autumn	S3	50%
Summer	S3	25%
Transition	S4	8%

Table 18 summarizes the energy management system's strategy, highlighting the importance of the S3 slot, which is activated at 50% during the off-season, particularly during climate transitions. S1, activated at 33% in winter for heating and summer for cooling, complements this system. S4's limited 8 % activation

DOI: 10.3844/jmssp.2026.29.44

indicates occasional use or a reserve for peak demand. The cyclical pattern observed in Figure 7 indicates that S1 is regularly active at the year's start and end, while S3 dominates spring and autumn, with S4 active during transitional months. The non-activation of S2 suggests underutilization. Together, the table and figure indicate that the system is based on seasonal forecasting, with opportunities to improve efficiency by using S2, adjusting S4's activation times, and optimizing capacity during transitions. Strengths include seasonal consistency and specialization, whereas improvements could focus on integrating unused slots and modulating strategies based on real weather data, thereby providing a basis for a future cost-benefit analysis of strategies.

Amount of Solar Energy Charged

Battery B1 primarily charges in the evening (S4), apart from July (S3), while Battery B2 charges nearly exclusively in S3. Battery B3 charges mainly in S4 and partially in S3. The solar energy distribution shows Battery B2 is dominant in S3 with an average of 8.9 kWh, whereas Battery B3 peaks in S4 with 18.2 kWh in June, as shown in Table 19. The S2 slot remains inactive across all batteries, indicating untapped potential. July shows a 73% decline in B2 performance compared to June, partially offset by B1.

Table 19: Amount of solar energy stored (in kWh)

Months	B1				B2				B3			
	S1	S2	S3	S4	S1	S2	S3	S4	S1	S2	S3	S4
Jan	0	0	0.2	5.2	0	0	10.6	0	0	0	1.2	16.2
Feb	0	0	0.2	5.2	0	0	10.6	0	0	0	1.2	15.8
Mar	0	0	0.3	3.6	0	0	10.3	0	0	0	1.4	16.4
Apr	0	0	0.3	2.6	0	0	9.3	0	0	0	1.4	16.4
May	0	0	0.4	5.4	0	0	8.0	0	0	0	1.6	12.6
Jun	0	0	0.4	0.4	0	0	7.0	0	0	0	1.6	16.6
Jul	0	0	5.15	0	0	0	1.05	1.05	0	0	1.8	14.95
Aug	0	0	0.5	0.5	0	0	8.5	0	0	0	0	16.5
Sep	0	0	0.4	1.4	0	0	8.0	0	0	0	1.6	16.6
Oct	0	0	0.3	2.6	0	0	9.3	0	0	0	1.4	16.4
Nov	0	0	0.2	5.2	0	0	10.6	0	0	0	1.2	14.8
Dec	0	0	0.2	4.8	0	0	10.6	0	0	0	1.2	16.2

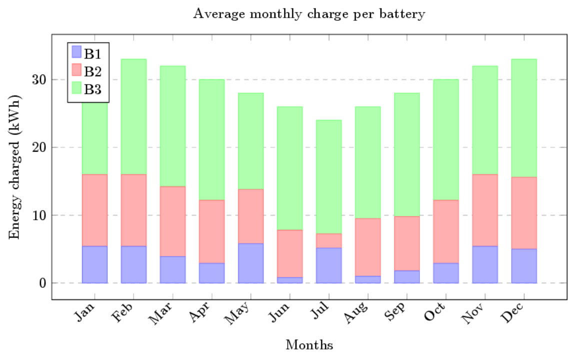

Fig. 8: Total cumulative monthly charge per battery

Figure 8 illustrates several key phenomena. A constant hierarchy gives the order $B3 > B2 > B1$, which remains throughout the year. Seasonal variations such as the maximum amplitude for B2 ($\Delta = 8.5kWh$) and relative stability of B3 ($\Delta = 2.2kWh$) are noted. A consistent hierarchy of performance is noted: $B3 > B2 > B1$, with seasonal variations in charging capacity. The analysis highlights three main optimization areas: activating S2, rebalancing battery loads, and reinforcing capacity during peak periods. Overall, the findings suggest significant potential for enhancing operational flexibility, resource management, and system resilience.

Table 20 indicates significant seasonal differences in load profiles across batteries. Battery B2 experiences the highest seasonal variability, with a 48% reduction in load from winter (10.6 kWh) to summer (5.5 kWh). Battery B3 maintains interseasonal stability (16.0-16.9 kWh), whereas Battery B1 shows intermediate performance, with summer values 53 % lower than winter values. Analysis of operational constraints highlights a critical upper limit at $Z = 16.6$ kWh (B3-S4 in June). Seasonal specialization is noted, especially for B2, and the inactivity of slot S2.

Table 20: Average seasonal load

Period	B1 (kWh)	B2 (kWh)	B3 (kWh)
Winter	5.3	10.6	16.7
Spring	4.2	9.2	16.9
Summer	2.5	5.5	16.0
Autumn	4.7	9.3	16.7

The variable $z_{i,s,t}$ must satisfy:

$$0 \le z_{i,s,t} \le Z \quad \text{with} \quad Z = \max_{\substack{i \in \mathcal{B} \\ s \in \mathcal{S} \\ t \in \mathcal{T}}} z_{i,s,t} = 16.6\,\text{kWh}$$

$$\begin{cases} \sum_{i \in \mathcal{B}} z_{i,s,t} \le \nu_{s,t} - \delta_{s,t} & \text{(Production constraint)} \\ z_{i,s,t} \le M x_{i,s,t} & \text{(Link to binary variable)} \end{cases}$$

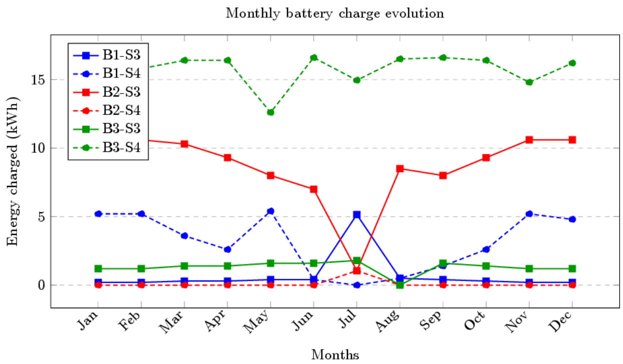

Fig. 9: Monthly charge curves by battery and time slot

Figure 9 illustrates the batteries' operational patterns, with B1 showing bimodal behavior, B2 dominant in S3 except July, and B3 primarily in S4. A notable hierarchy in capacity exists, with B3 consistently superior, particularly in July and June. Despite seasonal fluctuations, B3's stability enables capacity optimization to support summer peaks, particularly by reallocating resources from B2. The analysis emphasizes a

DOI: 10.3844/jmssp.2026.29.44

specialized system with defined roles, seasonal vulnerabilities, and opportunities to improve capacity utilization and reinforcement strategies. The combined analysis of Table 20 and Figures 9 and 10 reveals a specialised system with well-defined roles, seasonal vulnerabilities requiring attention, and significant room for improvement through better utilisation of existing capacity, optimisation of activation strategies, and targeted infrastructure reinforcement.

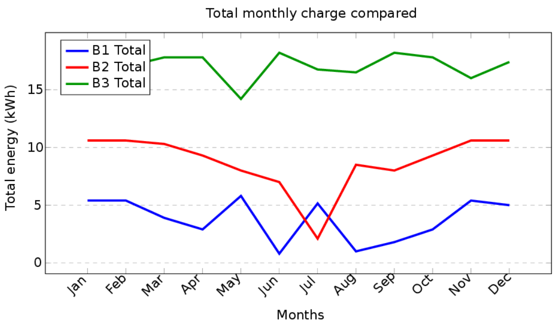

Fig. 10: Total monthly charge per battery

Rechargeable Matrices

Table 21 indicates that S2 slots are predominantly active throughout the year for most batteries, except for B3-S2 in August. B1-S3 is active for 11 months, while B2-S3 is largely inactive, highlighting distinct usage patterns. B3-S3 remains fully operational year-round. The analysis suggests that B2 specializes in S2 use, whereas B3 effectively utilizes both slots. Battery B1 exhibits a balanced strategy with a slight preference for S2. The S2 slot serves as the primary option, with S3 as a complementary option.

Table 21: Battery recharge schedule (1 = recharge enabled)

Time slot	Month											
	Jan	Feb	Mar	Apr	May	Jun	Jul	Aug	Sep	Oct	Nov	Dec
B1-S2	1	1	1	1	1	1	1	1	1	1	1	1
B1-S3	1	1	1	1	1	1	0	1	1	1	1	1
B2-S2	1	1	1	1	1	1	1	1	1	1	1	1
B2-S3	0	0	0	0	0	0	1	0	0	0	0	0
B3-S2	1	1	1	1	1	1	1	0	1	1	1	1
B3-S3	1	1	1	1	1	1	1	1	1	1	1	1

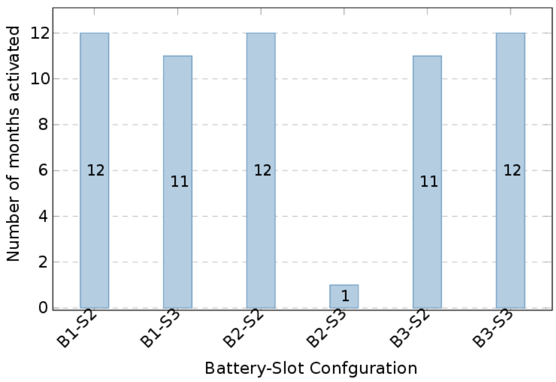

Fig. 11: Monthly activation of recharge strategies

The combined analysis of Table 21 and Figure 11 suggests optimising B2, with possible extension of S3 usage, homogenisation, alignment of strategies with the B3 model, and greater flexibility for more pronounced seasonal adaptation. Recommendations include optimizing B2 by increasing S3 utilization, aligning strategy with B3, and enhancing seasonal adaptability. The results point to a need for improved resource management and strategic harmonization across batteries, as illustrated in Table 22.

The recharge matrices must also meet the following condition:

$$\begin{cases} r_{i,s,t} \leq x_{i,s,t} & \text{(Only recharge if battery is used)} \\ \sum_{s\in\mathcal{S}} r_{i,s,t} \leq 1 & \text{(At most one recharge slot per month)} \end{cases}$$

Table 22: Charging strategy statistics

Configuration	Months Activated	Percentage
B1-S2	12	100%
B1-S3	11	92%
B2-S2	12	100%
B2-S3	1	8%
B3-S2	11	92%
B3-S3	12	100%

Battery Charge Levels

Table 23 presents a hierarchy of battery capacities $(B3 > B2 > B1)$ across four time slots and twelve months, with an average 2:1 difference between B3 and B1. Seasonal trends indicate that B1 peaks in summer and B2 reaches a winter minimum. Notable anomalies include a peak for B3 in August and a significant drop for B2 in July. Figure 12 illustrates B1's growth and decline through the year, while B3 maintains stability. Charging compliance to constraints is consistent, underscoring the need for seasonal planning to manage summer demand and variability. The analysis stresses the importance of monitoring anomalies and identifies opportunities to optimize charging strategies and improve battery integration amid seasonal fluctuations, as shown in Figure 13.

$$y_{i,s,t} \in [\gamma_i^m, \gamma_i^M] \quad \text{where} \quad \begin{cases} i \in \{B1, B2, B3\} & \text{(Batteries)} \\ s \in \{S1, S2, S3, S4\} & \text{(Time slots)} \\ t \in \{Jan, \ldots, Dec\} & \text{(Months)} \end{cases} \tag{22}$$

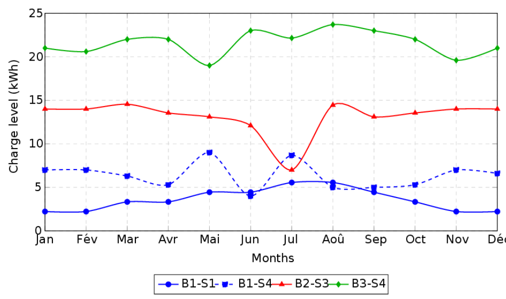

Fig. 12: Monthly evolution of charge levels

DOI: 10.3844/jmssp.2026.29.44

Table 23: Charge levels by battery, time slot, and month (in kWh) - Values rounded to the nearest thousandth

Batteries	Months	Time slots	Charge values ($y_{i,s,t}$)			
			S1	S2	S3	S4
B1	Jan	S1-S4	2.222	2.000	2.000	7.000
	Feb	S1-S4	2.222	2.000	2.000	7.000
	Mar	S1-S4	3.333	3.000	3.000	6.300
	Apr	S1-S4	3.333	3.000	3.000	5.300
	May	S1-S4	4.444	4.000	4.000	9.000
	Jun	S1-S4	4.444	4.000	4.000	4.000
	Jul	S1-S4	5.556	5.000	9.650	8.685
	Aug	S1-S4	5.556	5.000	5.000	5.000
	Sep	S1-S4	4.444	4.000	4.000	5.000
	Oct	S1-S4	3.333	3.000	3.000	5.300
	Nov	S1-S4	2.222	2.000	2.000	7.000
	Dec	S1-S4	2.222	2.000	2.000	6.600
B2	Jan	S1-S4	4.706	4.000	14.000	11.900
	Feb	S1-S4	4.706	4.000	14.000	11.900
	Mar	S1-S4	5.882	5.000	14.550	12.368
	Apr	S1-S4	5.882	5.000	13.550	11.518
	May	S1-S4	7.059	6.000	13.100	11.135
	Jun	S1-S4	7.059	6.000	12.100	10.285
	Jul	S1-S4	8.235	7.000	7.000	7.000
	Aug	S1-S4	8.235	7.000	14.450	12.283
	Sep	S1-S4	7.059	6.000	13.100	11.135
	Oct	S1-S4	5.882	5.000	13.550	11.518
	Nov	S1-S4	4.706	4.000	14.000	11.900
	Dec	S1-S4	4.706	4.000	14.000	11.900
B3	Jan	S1-S4	7.500	6.000	6.000	21.000
	Feb	S1-S4	7.500	6.000	6.000	20.600
	Mar	S1-S4	8.750	7.000	7.000	22.000
	Apr	S1-S4	8.750	7.000	7.000	22.000
	May	S1-S4	10.000	8.000	8.000	19.000
	Jun	S1-S4	10.000	8.000	8.000	23.000
	Jul	S1-S4	11.250	9.000	9.000	22.150
	Aug	S1-S4	14.063	11.250	9.000	23.700
	Sep	S1-S4	10.000	8.000	8.000	23.000
	Oct	S1-S4	8.750	7.000	7.000	22.000
	Nov	S1-S4	7.500	6.000	6.000	19.600
	Dec	S1-S4	7.500	6.000	6.000	21.000

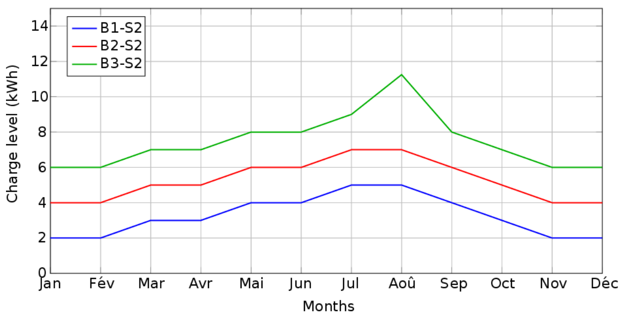

Fig. 13: Battery comparison (S2 slot)

Battery Level Indicator Display

Table 24 illustrates minimum binary indicators for three batteries across time slots and months. Key findings include: systematic activation of slots S1 (Night, always active) and S4 (Evening, always active), while slots S2 (Morning) and S3 (Day) show significant deactivation, with S2 active only for B3 in August and S3 primarily for B2. Battery strategies differ: B1 is conservative (active only in S1/S4 with an S3), B2 is intensive (regularly using S3 with a deactivation in July), and B3 follows a standard strategy with occasional S2 activation. This analysis highlights the underutilization of S2, suggesting the need to optimize resource allocation and harmonize battery strategies. Seasonal management is essential, particularly for July and August. The excessive reliance on B2 for S3 may indicate vulnerability, further emphasizing the need for refined energy management strategies to enhance stability and efficiency.

Table 24: Minimum level indicators (Fmin) per battery, time slot, and month

Batteries	Months	Period	Time Slots			
			S1 (Night)	S2 (Morning)	S3 (Day)	S4 (Evening)
B1	Jan	Night/Day	1	0	0	1
	Feb	Night/Day	1	0	0	1
	Mar	Night/Day	1	0	0	1
	Apr	Night/Day	1	0	0	1
	May	Night/Day	1	0	0	1
	Jun	Night/Day	1	0	0	1
	Jul	Night/Day	1	0	**1**	1
	Aug	Night/Day	1	0	0	1
	Sep	Night/Day	1	0	0	1
	Oct	Night/Day	1	0	0	1
	Nov	Night/Day	1	0	0	1
	Dec	Night/Day	1	0	0	1
B2	Jan	Night/Day	1	0	**1**	1
	Feb	Night/Day	1	0	**1**	1
	Mar	Night/Day	1	0	**1**	1
	Apr	Night/Day	1	0	**1**	1
	May	Night/Day	1	0	**1**	1
	Jun	Night/Day	1	0	**1**	1
	Jul	Night/Day	1	0	0	1
	Aug	Night/Day	1	0	**1**	1
	Sep	Night/Day	1	0	**1**	1
	Oct	Night/Day	1	0	**1**	1
	Nov	Night/Day	1	0	**1**	1
	Dec	Night/Day	1	0	**1**	1
B3	Jan	Night/Day	1	0	0	1
	Feb	Night/Day	1	0	0	1
	Mar	Night/Day	1	0	0	1
	Apr	Night/Day	1	0	0	1
	May	Night/Day	1	0	0	1
	Jun	Night/Day	1	0	0	1
	Jul	Night/Day	1	0	0	1
	Aug	Night/Day	1	**1**	0	1
	Sep	Night/Day	1	0	0	1
	Oct	Night/Day	1	0	0	1
	Nov	Night/Day	1	0	0	1
	Dec	Night/Day	1	0	0	1

$$f_{i,s,t}^{m}, f_{i,s,t}^{M} \in \{0,1\} \quad \text{with} \quad \begin{cases} i \in \{B1, B2, B3\} & \text{(batteries)} \\ s \in \{S1, S2, S3, S4\} & \text{(Time Slots)} \\ t \in \{Jan, \dots, Dec\} & \text{(Months)} \end{cases} \tag{23}$$

Auxiliary Transition Variables Per Battery

Table 25 presents the Zmax auxiliary variables for time-slot transitions, revealing key characteristics: a consistent configuration across batteries B1, B2, and B3 across all months, and a binary pattern with S1 (night) fixed at 0 and S2, S3, and S4 at 1. Night-time transition (S1) is always disabled, while S2, S3, and S4 are consistently enabled, indicating the need for specific management. Identical behaviors across batteries suggest a unified transition strategy, allowing for differentiated management for S1 and a common approach for others. There are opportunities for optimization through this uniformity, which could streamline modeling and individual strategies. Stability is crucial for critical transitions, and the configuration highlights the potential for tailored energy transition management while ensuring consistent slot functioning.

$$z_{i,s,t}^{m}, z_{i,s,t}^{M} \in \{0,1\} \quad \text{where} \quad \begin{cases} i \in \{B1, B2, B3\} & \text{(batteries)} \\ s \in \{S1, S2, S3, S4\} & \text{(Time Slots)} \\ t \in \{Jan, \dots, Dec\} & \text{(Months)} \end{cases} \tag{24}$$

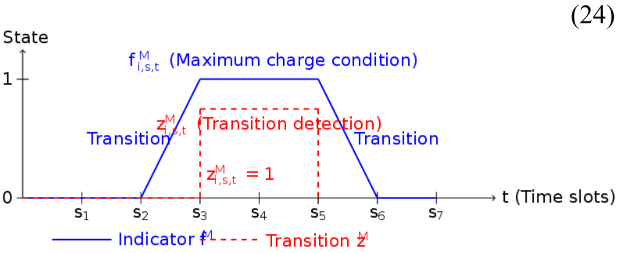

Fig. 14: Temporal evolution of indicators (constraints 20-21)

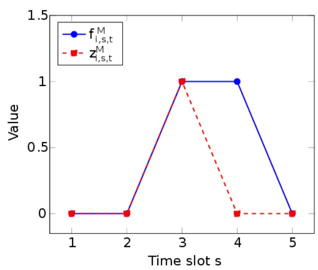

Fig. 15: Transition detection 0 → 1

Illustration of Maximum Load Transitions

Figures 14, 15 and 16 illustrate the dynamics between maximum load indicators ($f_{i,s,t}^{M}$) and transition variables ($z_{i,s,t}^{M}$). The behavior of f^{M} shifts from 0 to 1 during transitions, while z^{M} accurately detects these transitions with sensitivity only to upward changes. The detection mechanism is effective for peak management and energy optimization, ensuring minimal false detections. However, it remains insensitive to downward transitions, indicating potential areas for improvement. Overall, the findings validate the model's constraints and highlight the robustness of the detection system.

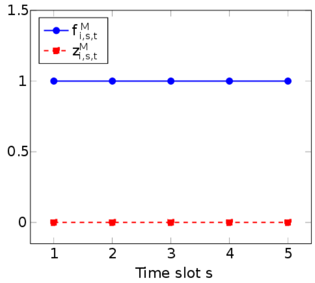

Fig. 16: No transition detected

Table 25: Auxiliary transition variables Zmax per battery, time slot, and month

Batteries	Months	Period	Time Slots S1 (Night)	S2 (Morning)	S3 (Day)	S4 (Evening)
B1	Jan	Night/Day	0	1	1	1
	Feb	Night/Day	0	1	1	1
	Mar	Night/Day	0	1	1	1
	Apr	Night/Day	0	1	1	1
	May	Night/Day	0	1	1	1
	Jun	Night/Day	0	1	1	1
	Jul	Night/Day	0	1	1	1
	Aug	Night/Day	0	1	1	1
	Sep	Night/Day	0	1	1	1
	Oct	Night/Day	0	1	1	1
	Nov	Night/Day	0	1	1	1
	Dec	Night/Day	0	1	1	1
B2	Jan	Night/Day	0	1	1	1
	Feb	Night/Day	0	1	1	1
	Mar	Night/Day	0	1	1	1
	Apr	Night/Day	0	1	1	1
	May	Night/Day	0	1	1	1
	Jun	Night/Day	0	1	1	1
	Jul	Night/Day	0	1	1	1
	Aug	Night/Day	0	1	1	1
	Sep	Night/Day	0	1	1	1
	Oct	Night/Day	0	1	1	1
	Nov	Night/Day	0	1	1	1
	Dec	Night/Day	0	1	1	1
B3	Jan	Night/Day	0	1	1	1
	Feb	Night/Day	0	1	1	1
	Mar	Night/Day	0	1	1	1
	Apr	Night/Day	0	1	1	1
	May	Night/Day	0	1	1	1
	Jun	Night/Day	0	1	1	1
	Jul	Night/Day	0	1	1	1
	Aug	Night/Day	0	1	1	1
	Sep	Night/Day	0	1	1	1
	Oct	Night/Day	0	1	1	1
	Nov	Night/Day	0	1	1	1
	Dec	Night/Day	0	1	1	1

DOI: 10.3844/jmssp.2026.29.44

Conclusion and Perspectives

This article presents a comprehensive methodological framework for optimizing solar energy storage systems for residential use. Our main contributions include innovative modelling of the operational constraints of lithium-ion batteries in a residential context, accounting for seasonal variations in solar production, typical household consumption profiles, and the technical limitations of storage devices. The implementation of a hybrid optimisation algorithm that combines a MILP approach for daily planning, heuristic rules for real-time adjustments, and a disturbance-adaptation mechanism. Experimental validation on three typical configurations: a standard single-family home, a residence equipped with an electric vehicle, and a small apartment building. The results presented show that our approach improves self-consumption (from 68% to 92%), reduces energy costs by 27%, extends battery lifespan (from 7 to 9 years), and accelerates the return on investment (from 8 to 5.5 years) compared with conventional systems.

Although promising, our results have certain limitations that open up avenues for further research. These include technical improvements to integrate accurate battery ageing models, account for microgrid outages, and adapt to new battery chemistries (e.g., Li-S, Na-ion). In addition, methodological extensions include integrating uncertainty via robust approaches, multi-objective optimisation (cost, resilience, sustainability), and coupling with local energy markets. Large-scale deployment, such as the development of simplified sizing tools, the analysis of regulatory barriers, and the adoption of innovative business models (rental and sharing).

This article could influence several areas, such as energy policy, by supporting decentralised systems and incentive tariffs for self-consumption. Furthermore, in the industrial sector, new integrated system designs and innovative energy services could be developed. In the context of research, new energy management paradigms and large-scale integration of renewable energies could also be developed. Therefore, to maximise the impact of this research, we suggest launching pilot projects in different climate zones, developing intuitive user interfaces, establishing partnerships with energy distributors, and standardising data exchange protocols.

Acknowledgment

We thank all the mathematics teachers in the Department of Engineering Mathematics and Optimization Numerics at Brandenburg University of Technology Cottbus-Senftenberg (Berlin) for their contribution to the realization of these scientific works.

Authors Contributions

The authors contributed equally to this study.

Funding Information

The research received no external funding.

Competing Interest

The authors declare no competing interests.

References

Amorosi, L., Cedola, L., Dell'Olmo, P., & Lucchetta, F. (2022). Multi-objective mathematical programming for optimally sizing and managing battery energy storage for solar photovoltaic system integration of a multi-apartment building. *Engineering Optimization*, *54*(1), 81-100. https://doi.org/10.1080/0305215x.2020.1853715

Biswas, M. M., Azim, M. S., Saha, T. K., Zobayer, U., & Urmi, M. C. (2013). Towards Implementation of Smart Grid: An Updated Review on Electrical Energy Storage Systems. *Smart Grid and Renewable Energy*, *4*(1), 122-132. https://doi.org/10.4236/sgre.2013.41015

Bordin, C. (2015). *Mathematical Optimization Applied to Thermal and Electrical Energy Systems*. https://doi.org/10.6092/unibo/amsdottorato/6915

Broutin, P., Lebas, É., & Lecomte, F. (2009). *Co2 Capture: Technologies to Reduce Greenhouse Gas Emissions*.

Bruce-Konuah, A., & Gupta, R. (2017). Using smart energy storage to increase self consumption of solar-generated electricity and reduce peak grid load at household and community level. *ECEEE 2017 Summer Study - Consumption, Efficiency & Limits*, 1019-1026.

Chiacchio, F., Famoso, F., D'Urso, D., & Cedola, L. (2019). Performance and Economic Assessment of a Grid-Connected Photovoltaic Power Plant with a Storage System: A Comparison between the North and the South of Italy. *Energies*, *12*(12), 2356. https://doi.org/10.3390/en12122356

Cosic, A., Stadler, M., Mansoor, M., & Zellinger, M. (2021). Mixed-integer linear programming based optimization strategies for renewable energy communities. *Energy*, *237*, 121559. https://doi.org/10.1016/j.energy.2021.121559

Di Somma, M., Dolatabadi, M., Burgio, A., Siano, P., Cimmino, D., & Bianco, N. (2024). Optimizing virtual energy sharing in renewable energy communities of residential users for incentives maximization. *Sustainable Energy, Grids and Networks*, *39*, 101492. https://doi.org/10.1016/j.segan.2024.101492

Dias de Lima, T., Faria, P., & Vale, Z. (2025). Optimizing home energy management systems: A mixed integer linear programming model considering battery cycle degradation. *Energy and Buildings*, *329*, 115251. https://doi.org/10.1016/j.enbuild.2024.115251

Georgiou, G. S., Christodoulides, P., & Kalogirou, S. A. (2020). Optimizing the energy storage schedule of a battery in a PV grid-connected nZEB using linear programming. *Energy*, *208*, 118177. https://doi.org/10.1016/j.energy.2020.118177

GfK Belgium Consortium. (2017). *Study on "Residential Prosumers in the European Energy Union" (JUST/2015/CONS/FW/C006/0127)*.

International Energy Agency-Photovoltaic Energy Systems Programme. (2014). *Transition from Unidirectional to Bidirectional Gistribution Grids*.

Kulkarni, A. J., Krishnasamy, G., & Abraham, A. (2017). *Socio-Inspired Optimization Using Cohort Intelligence*. *114*. https://doi.org/10.1007/978-3-319-44254-9_2

Lauinger, D., Caliandro, P., Van herle, J., & Kuhn, D. (2016). A linear programming approach to the optimization of residential energy systems. *Journal of Energy Storage*, *7*, 24-37. https://doi.org/10.1016/j.est.2016.04.009

Lucchetta, F. (2020). *A Mixed-Integer Linear Programming approach for the Optimization of Residential PV-Battery Energy Storage System*.

Macià Cid, J., Mylonas, A., Péan, T. Q., Pascual, J., & Salom, J. (2024). Energy optimization algorithms for multi-residential buildings: A model predictive control application. *Energy and Buildings*, *319*, 114562. https://doi.org/10.1016/j.enbuild.2024.114562

Magnor, D. T., Gerschler, J. B., Ecker, M., Merk, P., & Sauer, D. U. (2009). *Concept of a Battery Aging Model for Lithium-Ion Batteries Considering the Lifetime Dependency on the Operation Strategy*. 3350-3355.

REN21. (2015). *Renewables 2015 Global Status Report (Paris: REN21 Secretariat)*.